



# PgpP is a broadly conserved phosphatase required for phosphatidylglycerol lipid synthesis

Angelika Gründling<sup>a,b,1</sup> , Anna P. Brogan<sup>b</sup> , Michael J. James<sup>b</sup>, Fernando H. Ramirez-Guadiana<sup>b</sup> , Ian J. Roney<sup>b</sup> , Thomas G. Bernhardt<sup>b,c</sup> , and David Z. Rudner<sup>b</sup>

Edited by Thomas Silhavy, Princeton University, Princeton, NJ; received September 14, 2024; accepted December 16, 2024

The cytoplasmic membrane of bacteria is composed of a phospholipid bilayer made up of a diverse set of lipids. Phosphatidylglycerol (PG) is one of the principal constituents and its production is essential for growth in many bacteria. All the enzymes required for PG biogenesis in *Escherichia coli* have been identified and characterized decades ago. However, it has remained poorly understood how gram-positive bacteria perform the terminal step in the pathway that produces this essential lipid. In *E. coli*, this reaction is mediated by three functionally redundant phosphatases that convert phosphatidylglycerophosphate (PGP) into PG. Here, we show that homologs of these enzymes in *Bacillus subtilis* are not required for PG synthesis. Instead, we identified a previously uncharacterized *B. subtilis* protein, YqeG (renamed PgpP), as an essential enzyme required for the conversion of PGP into PG. Expression of *B. subtilis* or *Staphylococcus aureus* PgpP in *E. coli* lacking all three Pgp enzymes supported the growth of the strain. Furthermore, depletion of PgpP in *B. subtilis* led to growth arrest, reduced membrane lipid staining, and accumulation of PGP. PgpP is broadly conserved among Firmicutes and Cyanobacteria. Homologs are also present in yeast mitochondria and plant chloroplasts, suggesting that this widely distributed enzyme has an ancient origin. Finally, evidence suggests that PgpP homologs are essential in many gram-positive pathogens and thus the enzyme represents an attractive target for antibiotic development.

*Bacillus subtilis* | phospholipid synthesis | PGP phosphatase | phosphatidylglycerol

Membranes are essential biological structures that compartmentalize cells and organelles. In bacteria, the cytoplasmic membrane is principally composed of phospholipids. Their synthesis has been best characterized in the gram-negative bacterium *Escherichia coli*. Seminal studies from the Kennedy group in the 1960s and 1970s established the underlying principles and biosynthetic pathways of the major phospholipids (reviewed in refs. 1 and 2). These and subsequent studies led to the identification and biochemical characterization of all the enzymes required for the production of phospholipids in *E. coli* (reviewed in ref. 2). The Kennedy pathway and most of the biosynthetic enzymes are broadly conserved in bacteria (reviewed in ref. 2). Despite over a century of research on phospholipid synthesis, there are still important gaps in our understanding of their biogenesis in bacteria other than *E. coli*. Here, we report the results of a 15-y quest by the first author to define the complete lipoteichoic acid (LTA) synthesis pathway in Firmicutes (3, 4) that identified the missing enzyme required for the synthesis of phosphatidylglycerol (PG) in gram-positive bacteria.

The major phospholipids in the cytoplasmic membrane of the gram-positive model organism *Bacillus subtilis* are the zwitterionic phospholipid phosphatidylethanolamine (PE), the anionic lipid PG and the neutral lipids: diacylglycerol (DAG) and glycolipids (5–7). The synthesis of these lipids begins with the production of a common precursor, phosphatidic acid (PA). In *B. subtilis* PA is produced by the enzymes PlsX, PlsY, and PlsC (Fig. 1A) (reviewed in ref. 8). PA is then converted to CDP-DAG by the broadly conserved enzyme CdsA (Fig. 1A). CDP-DAG serves as the precursor for the synthesis of both PE and PG. PE is an abundant lipid in *B. subtilis* membranes, yet cells unable to produce this lipid are viable and show only minor growth defects (5). On the other hand, PG, which is also required for synthesis of the membrane-anchored cell wall polymer LTA, is essential in *B. subtilis* and many other bacteria, including *E. coli* (9–11). PgsA catalyzes the first committing step in the PG lipid synthesis pathway and converts CDP-DAG into phosphatidylglycerophosphate (PGP) (12) (Fig. 1A). A phosphatase is then required to convert PGP into PG. In *E. coli*, three distinct phosphatases, PgpA, PgpB, and PgpC catalyze the conversion of PGP to PG (13, 14). The membrane-anchored enzyme, PgpA, is the primary PGP phosphatase in *E. coli* and the founding member of

## Significance

Despite a century of active research focused on the identification and characterization of enzymes required for phospholipid biosynthesis, it has remained unclear how gram-positive bacteria complete the synthesis of the essential membrane component phosphatidylglycerol (PG). Here, we demonstrate that the broadly conserved phosphatase, PgpP, catalyzes the terminal step of the PG synthesis pathway in gram-positive bacteria. PgpP is likely essential in many gram-positive pathogens and therefore represents an attractive target for antibiotic development.

Author affiliations: <sup>a</sup>Section of Molecular Microbiology and Centre for Bacterial Resistance Biology, Department of Infectious Disease, Imperial College London, London SW7 2AZ, United Kingdom; <sup>b</sup>Department of Microbiology, Blavatnik Institute, Harvard Medical School, Boston, MA 02115; and <sup>c</sup>HHMI, Chevy Chase, MD 20815

Author contributions: A.G., T.G.B., and D.Z.R. designed research; A.G. performed research; A.G., A.P.B., M.J.J., and I.J.R. contributed new reagents/analytic tools; A.G., M.J.J., F.H.R.-G., T.G.B., and D.Z.R. analyzed data; and A.G. and D.Z.R. wrote the paper.

The authors declare no competing interest.

This article is a PNAS Direct Submission.

Copyright © 2025 the Author(s). Published by PNAS. This article is distributed under [Creative Commons Attribution-NonCommercial-NoDerivatives License 4.0 \(CC BY-NC-ND\)](https://creativecommons.org/licenses/by-nc-nd/4.0/).

<sup>1</sup>To whom correspondence may be addressed. Email: [a.grundling@imperial.ac.uk](mailto:a.grundling@imperial.ac.uk).

This article contains supporting information online at <https://www.pnas.org/lookup/suppl/doi:10.1073/pnas.2418775122/-/DCSupplemental>.

Published January 27, 2025.

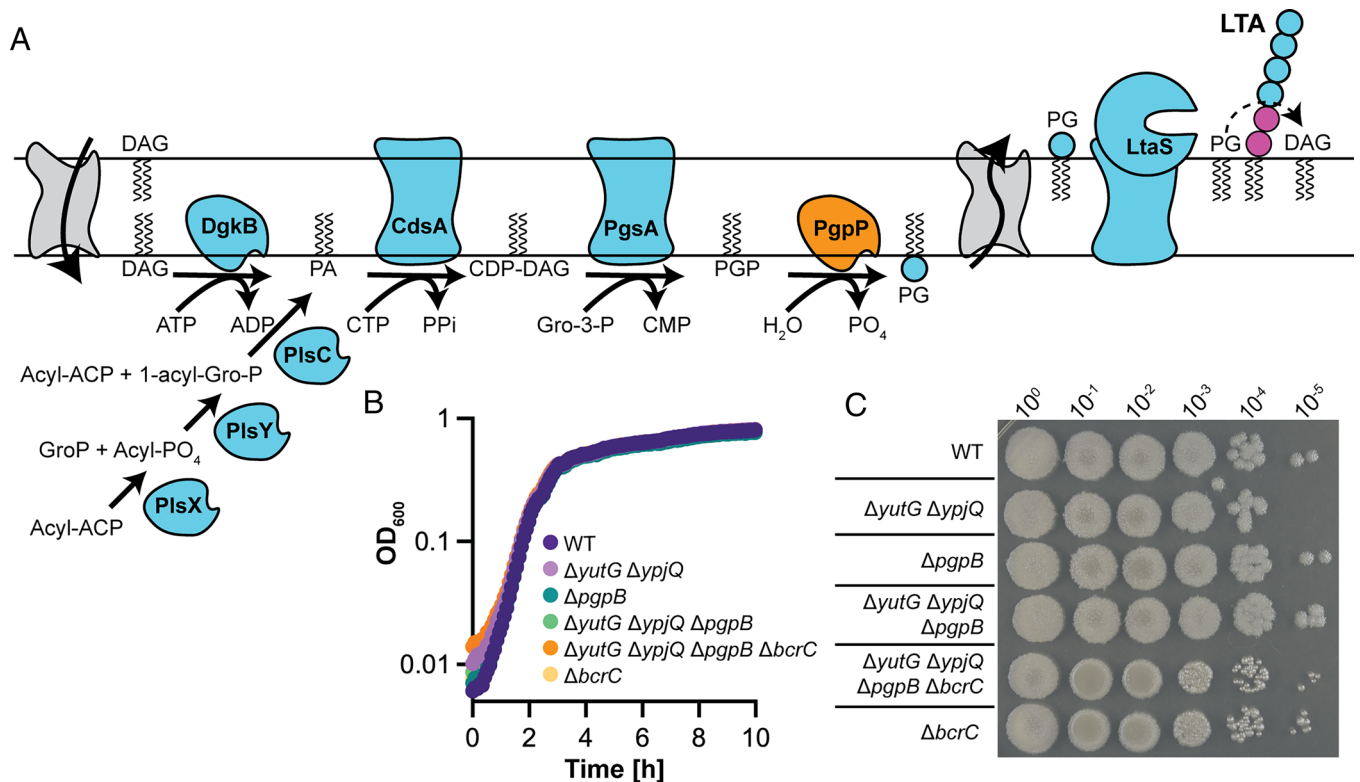


**Fig. 1.** *B. subtilis* strains lacking homologs of *E. coli* PgpA and PgpB are viable. (A) Schematic of the PG and LTA biosynthesis pathways in *B. subtilis*. Enzymes with known functions are shown in blue. The PGP phosphatase, PgpP (formally, YqeG) that catalyzes the terminal step in PG synthesis and identified in this study is shown in orange. The flippase(s) required to transport PG and DAG across the membrane (shown in gray) are unknown. (B) Growth curves of WT and the indicated single, double, triple, and quadruple mutants. (C) Photograph of spot-dilutions of the indicated strains on LB agar plates. The growth curve and spot-dilutions are representative results from one of four biological replicates.

the PgpA family of enzymes (13, 14). PgpB belongs to the PAP2 family of membrane-embedded phosphatases with an extracellular catalytic site. PgpB has also been found to dephosphorylate undecaprenylpyrophosphate (UndPP) to aid in the recycling of the lipid carrier used for the biogenesis of surface glycans (15). PgpC is a member of the haloacid dehydrogenase (HAD) superfamily and is a cytoplasmic phosphatase. *E. coli* strains with single and double mutants in *pgpA*, *pgpB*, and *pgpC* are viable. However, a strain lacking all three genes is unable to grow (13, 14), consistent with the essentiality of PG. A PgpB homolog (also known as YodM) has been identified in *B. subtilis*. When overexpressed, the PgpB (YodM) enzyme can rescue the growth of a *B. subtilis* mutant with deletions in *bcrC* and *uppP* coding for the two main UndPP phosphatases (16). Hence, PgpB (YodM) can function similarly to the *E. coli* PgpB homolog as minor UndPP phosphatase when overexpressed (16). Importantly, PgpB has also been found to convert PGP to PG in vivo and in vitro (17). However, *pgpB* is not essential in *B. subtilis* (16, 17), indicating that additional PGP phosphatases must exist.

In this study, we identify YqeG (renamed PgpP) as the missing PGP phosphatase in *B. subtilis*. Unlike the functional redundancy observed in *E. coli*, we find that *pgpP* is essential, indicating that it is the major PGP phosphatase in *B. subtilis*. PgpP is a HAD superfamily member, but it is not homologous to the *E. coli* PgpC protein. Interestingly, PgpP is more closely related to enzymes found in plant chloroplasts and yeast mitochondria, suggesting an ancient origin. Importantly, transposon-sequencing (Tn-Seq) screens suggest that *pgpP* is also essential in several important gram-positive pathogens, including *Staphylococcus aureus* (18), *Listeria monocytogenes* (19), *Enterococcus faecalis* (20), and

*Streptococcus pneumoniae* (21), making it an attractive target for antibiotic development.

## Results

***B. subtilis* Homologs of PgpA and PgpB Are Not Critical for PG Synthesis in *B. subtilis*.** In *B. subtilis*, PgpB (YodM) has been shown to convert PGP to PG but the gene is not essential for growth (16, 17). The functional redundancy of the phosphatases required to convert PGP to PG in *E. coli*, motivated us to search for additional enzymes that function in addition to the PgpB protein in this pathway. We used DELTA\_BLAST (22) to search the *B. subtilis* 168 genome using *E. coli* PgpA, PgpB, and PgpC protein sequences as queries. This analysis identified two potential PgpA homologs, BSU\_32280 (YutG) and BSU\_21830 (YpjQ), and two potential PgpB homologs BSU\_19650, (PgpB/YodM) and the UndPP phosphatase BSU\_36530 (BcrC) (23, 24) (SI Appendix, Table S1). There were 17 *B. subtilis* proteins identified as potential homologs of PgpC (SI Appendix, Table S1). However, because the highest confidence hits were ion transporter ATPases, these proteins were not investigated further.

To investigate whether the PgpA or PgpB homologs were required for PG synthesis, we constructed combinations of deletion mutants and assessed their growth and viability. Single, double, and triple mutants with deletions in *yutG*, *ypjQ*, and *pgpB* were all viable and grew like wild-type (WT) (Fig. 1 B and C). We also constructed the quadruple mutant with *bcrC* to test whether BcrC moonlights as PGP phosphatase. The quadruple mutant was also viable and grew similarly to WT in liquid culture (Fig. 1B). A modest growth defect of the quadruple mutant was

observed on agar plates, which phenocopied the growth defect of the  $\Delta bcrC$  single mutant (Fig. 1C). This phenotype was likely caused by the reduced conversion of UndPP to undecaprenyl phosphate (UndP) for lipid carrier recycling. These data suggested that *B. subtilis* possesses one or more additional PGP enzymes. To identify these potential phosphatases, we performed a synthetic lethal screen in the quadruple mutant using Tn-Seq. We generated diverse transposon libraries in WT, the quadruple mutant, and the *bcrC* single mutant and then mapped the insertion sites by next-generation sequencing. Strikingly, there were no genes in which transposons were underrepresented in the quadruple mutant compared to the *bcrC* control that resembled potential phosphatases (Dataset S1). These results led us to hypothesize that there is either more than one additional PGP phosphatase in *B. subtilis* or, unlike *E. coli*, a single essential enzyme is required for this step.

**Identification of a Gram-Positive Gene That Rescues the Growth of an *E. coli* *pgp* Mutant.** To screen for enzymes in gram-positive bacteria that can catalyze the conversion of PGP to PG, we took advantage of a conditional *pgp* *E. coli* strain YL24 pMAK-C (14). This strain lacks the native *pgpA*, *pgpB*, and *pgpC* genes and contains *pgpC* expressed under the control of an arabinose-inducible promoter on a temperature-sensitive plasmid. At low temperature in the presence of arabinose the strain is viable. However, under restrictive conditions (43 °C in the absence of inducer) the strain dies. Plasmid libraries containing *S. aureus* genomic DNA (gDNA) fragments that were constructed as part of a genetics course were introduced into the *E. coli* YL24 pMAK-C. Several transformants were obtained that rescued growth at the nonpermissive condition. The plasmids were isolated from these transformants and the sequence of the inserts determined.

Strikingly, many of the inserts mapped to a single chromosomal region in the *S. aureus* genome (SI Appendix, Fig. S1). Analysis of the insert boundaries and the predicted function of encoded proteins in this region identified SAOUHSC\_01701 (*yqeG*) as the most likely gene rescuing the growth of the *E. coli* PG synthesis mutant. The *yqeG* gene is part of a conserved operon and encodes an uncharacterized protein that belongs to the haloacid dehalogenase (HAD) IIIA-type phosphatase family (Fig. 2A). Importantly, *B. subtilis* encodes a homolog with 59% sequence identity to the *S. aureus* protein that is encoded in the same operon (Fig. 2A). Based on the experiments described below, we have renamed the *yqeG* gene, *pgpP* for PGP phosphatase.

To determine whether the *S. aureus* *pgpP<sub>SA</sub>* and the *B. subtilis* *pgpP<sub>BS</sub>* genes were sufficient to support growth of the *E. coli* *pgp* triple mutant, these genes were cloned into a plasmid with a xylose-regulated promoter. As positive controls, plasmids for expression of the *E. coli* *pgpA<sub>EC</sub>* and *pgpC<sub>EC</sub>* genes were also constructed and all four plasmids introduced into the *E. coli* strain YL24 pMAK-C along with the empty vector (EV) as a negative control. Expression of all four genes, *pgpA<sub>EC</sub>*, *pgpC<sub>EC</sub>*, *pgpP<sub>SA</sub>*, and *pgpP<sub>BS</sub>*, supported growth at the restrictive temperature, while a strain containing the EV control was unable to grow (Fig. 2B). These data strongly suggest that the *S. aureus* and *B. subtilis* *pgpP* genes encode functional PGP phosphatases.

**PgpP Is Essential for Growth of *B. subtilis* and Depletion Leads to Reduced Membrane Staining.** Based on Tn-Seq experiments and the Subtiwiki website, *pgpP* (*yqeG*) is an essential gene and encodes for one of 16 HAD superfamily enzymes (25). Consistent with this designation, all our attempts to delete the *pgpP* gene in *B. subtilis* were unsuccessful, as reported previously (26). Accordingly, we constructed a strain with inducible *pgpP* expression by placing

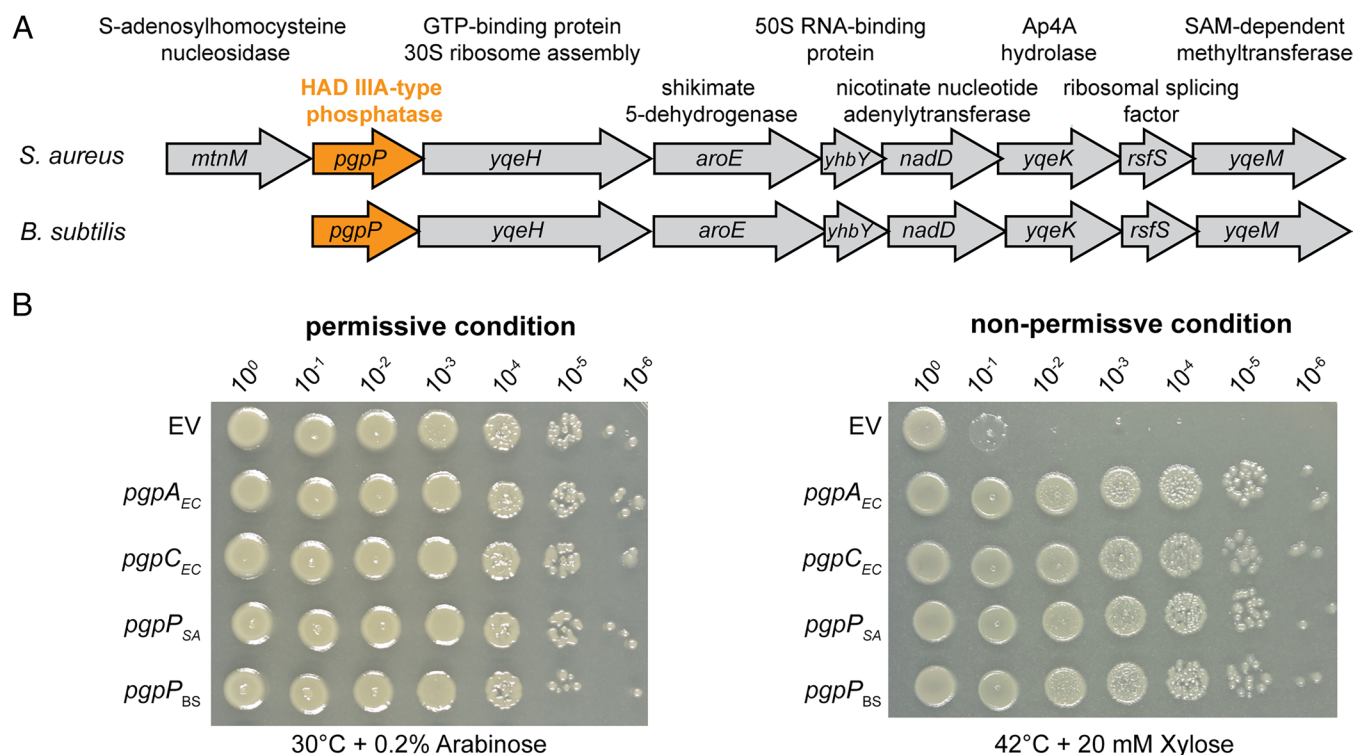


**Fig. 2.** The *S. aureus* and *B. subtilis* *pgpP* gene can rescue an *E. coli* *pgp* depletion strain. (A) Schematic of the genomic loci containing *pgpP* in *S. aureus* and *B. subtilis*. The operons containing *pgpP* (formally, *yqeG*) are depicted with genes drawn approximately to scale and gene names and protein function indicated. (B) Spot dilutions of *E. coli* strain YL24 pMAK-C containing the EV pCB095 or derivatives with *E. coli* *pgpA<sub>EC</sub>* or *pgpC<sub>EC</sub>*, *S. aureus* *pgpP<sub>SA</sub>* or *B. subtilis* *pgpP<sub>BS</sub>*. Strains were serially diluted and spotted onto an LB agar plate containing arabinose and incubated at 30 °C (permissive condition) or LB agar containing xylose and incubated at 42 °C (nonpermissive condition). At 42 °C bacteria can only grow if a functional PGP phosphatase is supplied on the pCB095 plasmid. Representative images from five independent experiments are shown.

the *pgpP* gene under control of an IPTG-regulated promoter and inserting the fusion at an ectopic site in the *B. subtilis* genome. Next, the *pgpP* gene at the native locus was deleted in this strain in the presence of IPTG (Fig. 3A). In the presence of inducer, the inducible *pgpP* strain (*i-pgpP*) grew similar to WT (Fig. 3B). However, the strain stopped growing 2 to 3 h after removal of IPTG (Fig. 3B). The growth defect was even more pronounced when the cultures were back diluted a second time following 3 h of growth without inducer (SI Appendix, Fig. S2).

To investigate whether the essentiality of *pgpP* was due to an inability to convert PGP to PG, we tested whether *pgcA*<sub>EC</sub> and *pgpC*<sub>EC</sub> could support growth of the mutant strain. To this end, *pgcA*<sub>EC</sub> and *pgpC*<sub>EC</sub> were placed under the control of a xylose-inducible promoter and introduced into the *i-pgpP* strain (Fig. 3C). Expression of either enzyme fully complemented the growth of this strain in the presence of xylose but absence of IPTG (Fig. 3D). Thus, the mutant is likely impaired in PGP phosphatase activity. Finally, and as expected, reintroduction of the *B. subtilis* *pgpP*<sub>BS</sub> or *S. aureus* *pgpP*<sub>SA</sub> genes also supported growth of the *B. subtilis* *i-pgpP* mutant in the presence of xylose but absence of IPTG (Fig. 3D).

To investigate whether depletion of PgpP leads to any cytological phenotypes, we analyzed exponentially growing cultures of WT and the depletion mutant before and 3 h after the removal of IPTG. The cells were stained with the membrane dye TMA-DPH and the membrane-impermeable DNA dye propidium iodide (PI) that only stains cells with membrane integrity defects and then visualized the bacteria by phase-contrast and fluorescence microscopy. In the presence of IPTG, the PgpP depletion strain looked indistinguishable from WT (Fig. 3E). Upon depletion of PgpP for 3 h the cells maintained their rod shape, but the number of cells with membrane integrity defects, as assayed by PI staining, increased. The number of PI-positive cells drastically increased when the bacteria were viewed 5 h after removal of the inducer (SI Appendix, Fig. S3). In addition, we observed already at the 3 h time point a reproducible reduction in TMA-DPH fluorescence and less “patchy” staining in the mutant (Fig. 3E). These findings are consistent with a defect in phospholipid biogenesis upon depletion of PgpP.

**Conserved Active-Site Aspartic Acid Residues Are Required for PgpP Function.** Using the *B. subtilis* PgpP AlphaFold2 model (AF-P54452-F1-model v4) (27, 28) to query the Foldseek server (29), we identified the yeast mitochondrial Gep4 protein as a potential PgpP homolog. The two predicted structures aligned with a Match align score of 95.5 and an RMSD of 2.442 Å (Fig. 4A). Gep4 has been shown to function as a PGP phosphatase in yeast mitochondria (30), providing additional support for the idea that PgpP is the missing PGP phosphatase in gram-positive bacteria.

Based on a sequence alignment between PgpP proteins and Gep4, aspartic acid residues 34 and 36 in *B. subtilis* PgpP were predicted to be part of a conserved active site motif hhhDxDx, where h indicates hydrophobic amino acids and x any amino acid (SI Appendix, Fig. S4) (30, 31). Both aspartic acids are in a recessed pocket within the predicted PgpP structure (Fig. 4A). To test whether these residues are required for PgpP function, we separately substituted the aspartic acid (D) for asparagine (N) at each position in the context of a functional PgpP-His fusion. Expression of WT PgpP or PgpP-His from a xylose inducible promoter supported growth of the *i-pgpP* mutant strain in the presence of xylose and absence of IPTG, both on agar plates as well as in liquid culture (Fig. 4B and SI Appendix, Fig. S5A). By contrast, expression of PgpP<sub>D34N</sub>-His or PgpP<sub>D36N</sub>-His did not complement the mutant and these strains behaved identical to the EV control strain

(Fig. 4B and SI Appendix, Fig. S5A). Importantly, both proteins were produced at levels similar to PgpP-His (Fig. 4C and SI Appendix, Fig. S5B). Furthermore, a strain producing lower levels of the PgpP-His protein achieved by propagating the strain in LB medium supplemented with lower xylose concentrations of 0.4 mM or 1.0 mM, was still able to grow in the absence of IPTG (SI Appendix, Fig. S5). These data show that the inability of the PgpP<sub>D34N</sub>-His or PgpP<sub>D36N</sub>-His variants to support growth was not due to protein instability or reduced protein production. Thus, the catalytic activity of PgpP is essential for growth. Taken together, these data provide additional support for the idea that PgpP, like Gep4, is a PGP phosphatase.

#### PGP Accumulates in *B. subtilis* Membranes upon PgpP Depletion.

To further test the model that PgpP converts PGP to PG in vivo, we analyzed the lipid profiles in WT and the PgpP depletion mutant. Total membrane lipids were extracted from WT and the depletion strain grown in LB medium in the presence and absence of IPTG. The lipids were resolved by thin-layer chromatography (TLC) using conditions that were previously used to visualize PGP derived from yeast mitochondrial lipid extracts prepared from a *gcp4* mutant (30). The membrane lipid profiles of the WT *B. subtilis* strain and the PgpP depletion strain grown in the presence of IPTG were indistinguishable (Fig. 5A). However, the lipid profile from cells depleted of PgpP had a slower migrating species. A similar slower migrating lipid band was previously observed in extracts from the *gcp4* mutant (30) suggesting that the lipid in the *B. subtilis* PgpP depletion strain is PGP. In a complementary experiment, we performed a TLC analysis with a different mobile phase that was unable to resolve PG and PGP, but allowed us to assign most lipids in the chromatogram (32). We observed clear differences in the lipid profile for the strain depleted of PgpP compared to WT that are consistent with impaired conversion of PGP to PG (SI Appendix, Fig. S6). For example, similar to the PgsA depletion control strain, which has a known defect in the PG lipid biosynthesis, the levels of cardiolipin, a lipid that is produced from two molecules of PG, were reduced in the PgpP depletion strain (SI Appendix, Fig. S6).

To directly address whether PGP accumulates in the PgpP depletion strain, total membrane lipid extracts were analyzed in the positive ion mode by LC-MS and LC-MS/MS. Since iso- and anteiso-C15:0, C16:0, and iso- or anteiso-C17:0 fatty acid chains are the most abundant fatty acids in *B. subtilis* lipids (6), we focused our analysis on the detection of PG and PGP lipids in which the combined fatty acid carbon chain length is C30:0, C31:0, or C32:0 (SI Appendix, Fig. S7). While clear peaks for masses corresponding to PG could be detected for both strains grown in the presence and absence of IPTG, mass signals corresponding to PGP were only abundant in the depletion strain in the absence of IPTG (Fig. 5B and SI Appendix, Fig. S8). To quantify the PGP/PG ratio we integrated and summed the PG and PGP peaks for the lipids which have a combined fatty acid carbon chain length of C30:0, C31:0, and C32:0. In WT, PGP is rapidly converted to PG, and hence the PGP/PG was low (<0.15). A similar ratio was observed in the depletion strain grown in the presence of IPTG. By contrast, the PGP/PG ratio was >1.5 in the PgpP depletion strain grown in the absence of inducer (Fig. 5C). Thus, PGP significantly accumulates upon depletion of PgpP. To confirm that the integrated mass peaks correspond to PG and PGP lipids, an LC-MS/MS experiment was performed. PG C15:0 C18:1-D7 (also referred to as PG 33:1-D7 when using the combined fatty acid carbon chain length) with a known chemical structure and mass was used as a control to determine the fragmentation pattern under our LC-MS/MS conditions (SI Appendix, Fig. S9 and Table S2). Mass fragments consistent

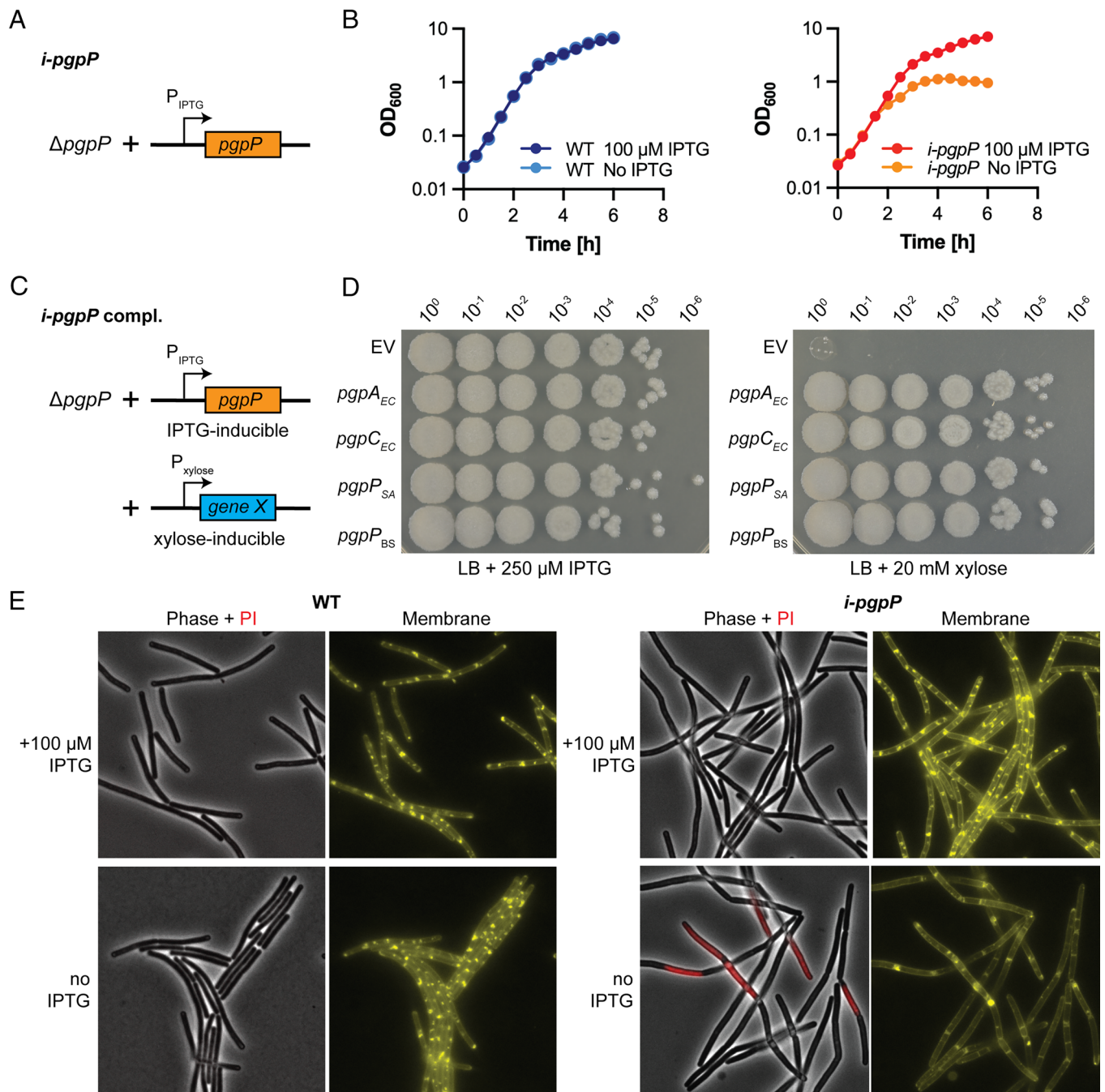


**Fig. 3.** PgpP is essential in *B. subtilis* and its depletion leads to membrane defects. (A) Schematic of the IPTG-inducible *pgpP* (*i-pgpP*) strain. (B) Growth curves of the indicated strains in the presence and absence of IPTG. The average reading and SD from three experiments were plotted. (C) Schematic of the IPTG-inducible *pgpP* (*i-pgpP*) strain with xylose-inducible complementation alleles. (D) Spot dilutions of the *i-pgpP* complementation strains constructed with the EV or with xylose-inducible *E. coli* *pgcA*<sub>EC</sub> or *pgpC*<sub>EC</sub>, *S. aureus* *pgpP*<sub>SA</sub> or *B. subtilis* *pgpP*<sub>BS</sub>. Strains were serially diluted and spotted onto LB agar plates containing 250  $\mu$ M IPTG (Left) or 20 mM xylose (Right). Representative images from three independent experiments are shown. (E) Representative phase-contrast and fluorescence images of WT *B. subtilis* and the *i-pgpP* strain. Cultures grown for 3 h in the presence or absence of IPTG were stained with PI and the membrane dye TMA-DPH and analyzed by phase-contrast and fluorescence microscopy. The PI fluorescence and phase-contrast images were overlaid to better visualize PI-positive cells (Phase + PI). TMA-DPH fluorescence (membrane) was false-colored yellow. The exposure time and scaling for all four PI and TMA-DPA images were identical. Representative images from one of three independent experiments are shown.

with the loss of the head group (Fragment 1) were observed, as well as masses consistent with the loss of the head group and either one or the other fatty acid chain (Fragments 2a and Fragment 2b) (SI Appendix, Fig. S10 and Table S3). The PG and PGP lipids with a combined fatty acid carbon chain length of C30:0, C31:0, and C32:0 isolated from WT and the PgpP depletion strains had masses consistent with an identical fragmentation pattern as the control PG lipid (SI Appendix, Figs. S7 and S11–S18 and Tables S2 and S3). Altogether, these data argue that PgpP is the primary PGP

lipid phosphatase in *B. subtilis* and, in its absence, the conversion of PGP to PG is blocked or drastically reduced leading to the accumulation of PGP.

## Discussion

Altogether our data indicate the PgpP is the long sought-phosphatase that converts PGP into PG in *B. subtilis* and completes the Kennedy pathway in this bacterium. In previous work,

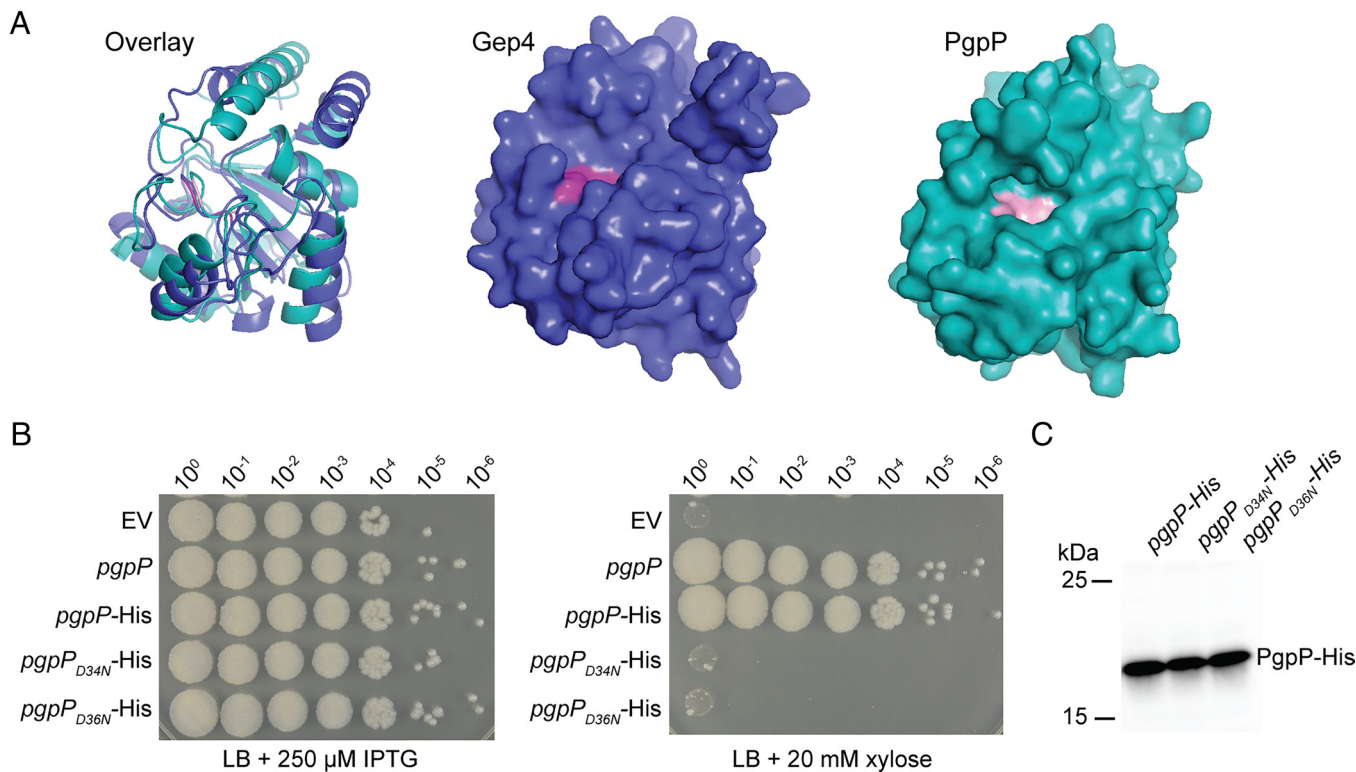


**Fig. 4.** The predicted structures of *B. subtilis* PgpP and the yeast mitochondrial PGP phosphatase Gep4 are similar and their active site aspartic acids are essential for function. (A) AlphaFold models of Gep4 and *B. subtilis* PgpP. *Left panel:* Overlay of the Gep4 (AF-P38812-F1-model\_v4) (purple) and *B. subtilis* PgpP (AF-P52254-F1-model\_v4) (cyan). *Middle and Right panels:* Surface representations of Gep4 and PgpP models with the active site aspartic acid residues highlighted in pink. The images were generated with PyMOL v 2.5.3. (B) Spot dilutions of the *i-pgpP* complementation strain constructed with an EV or with *pgpP*, *pgpP-His*, or the active site variants *pgpP<sub>D34N</sub>-His* or *pgpP<sub>D36N</sub>-His* expressed from a xylose-inducible promoter. Strains were serially diluted and spotted onto LB agar plates containing 250  $\mu$ M IPTG (*Left*) or 20 mM xylose (*Right*). Representative images from one of three independent experiments are shown. (C) Immunoblot analysis of PgpP-His or active site variants detected with an anti-His-tag antibody. Data from all strains analyzed are shown in *SI Appendix, Fig. S5* along with the SigA protein loading controls. A representative immunoblot from one of three biological replicates is shown.

it has been shown that the *B. subtilis* PgpB (YodM) protein can convert PGP to PG when expressed in *E. coli* or in vitro using *B. subtilis* membrane protein extracts (17). This influenced our original thinking that, like in *E. coli*, the PGP phosphatases in *B. subtilis* are likely to be redundant enzymes. However, here we show that PgpP is the main and essential PGP phosphatase in *B. subtilis* and that in its absence the activity of PgpB is not sufficient to support the growth of *B. subtilis*. The data obtained in the previous study suggested that PgpB is the main PGP phosphatase in *B. subtilis* since its activity accounted for 75% of the PGP phosphatase activity in *B. subtilis* membrane extracts (17). However, here it is of note that in contrast to PgpB, which is an integral membrane protein, the PgpP enzyme identified in this study, is not predicted to be an integral membrane protein. Instead, it is likely only peripherally attached to the membrane and thus providing a plausible explanation as to why its activity was missed in the previous PGP phosphatase activity assays in which detergent solubilized membrane protein extracts were used (17).

Using information from the COG database (33), which currently contains data from 1,187 bacterial and 122 archaeal genomes, we compared the distribution of PgpA (COG1267), the main PGP phosphatase in *E. coli* and PgpP (YqeG; COG02179), the main PGP phosphatase in *B. subtilis*. We also compared this information to the occurrence of PgsA, which catalyzes the first committed step in the PG lipid synthesis pathway and hence likely serves as a good indicator as to which bacteria can produce the PG lipid (Fig. 6A, *SI Appendix, Table S4*, and *Dataset S2*). This phylogenetic analysis indicates that PgpP homologs (YqeG; COG02179) are present in most Firmicutes and virtually all bacteria in the Bacilli class that includes *Bacillus*, *Staphylococcus*, *Listeria*, *Enterococcus*, and

*Streptococcus* sp. Although several of these bacteria also encode a PgpA homolog, based on our analysis of the PgpA-like proteins in *B. subtilis*, we suspect that many of these do not function as a PGP phosphatase or at least not as the main PGP phosphatase. In support of this idea, analysis of Tn-seq screens in *S. aureus*, *L. monocytogenes*, *E. faecalis*, and *S. pneumoniae* suggests that *pgpP* (*yqeG*) is essential in all of these organisms (18–21). Thus, we suspect that PgpP is the major PGP phosphatase in these bacteria. The enzyme therefore represents an attractive target for therapeutic development.

PgpP-type proteins are also present in most of the bacteria in the Clostridia, Thermotogae, Mollicutes, and Cyanobacteria phyla. In these phyla, PgpP is likely to be the main PGP phosphatase as PgpA-type proteins are often not present. Interestingly, PGP phosphatases from the same HAD superfamily are also present in algae and plant chloroplasts and have been shown to function as PGP phosphatases in *Chlamydomonas reinhardtii* and *Arabidopsis thaliana* (35–38). Thus, PgpP is likely an ancient enzyme that was present in ancestral endosymbiotic cyanobacteria that became chloroplasts.

PgpP is largely absent in Proteobacteria, and most of these bacteria have PgpA-type enzymes like *E. coli* (Fig. 6, *SI Appendix, Table S4*, and *Dataset S2*). The members of the Rhizobiales order within the Alphaproteobacteria, which lack both PgpA- and PgpP-type enzymes, represent an interesting exception. In addition, most bacteria belonging to the Chlamydiae and Actinobacteria phylum lack PgpA- and PgpP-type enzymes. Since these bacteria encode homologs of the committing PG synthesis enzyme PgsA, these observations raise the possibility that a fifth class of PGP phosphatase exists in these organisms.

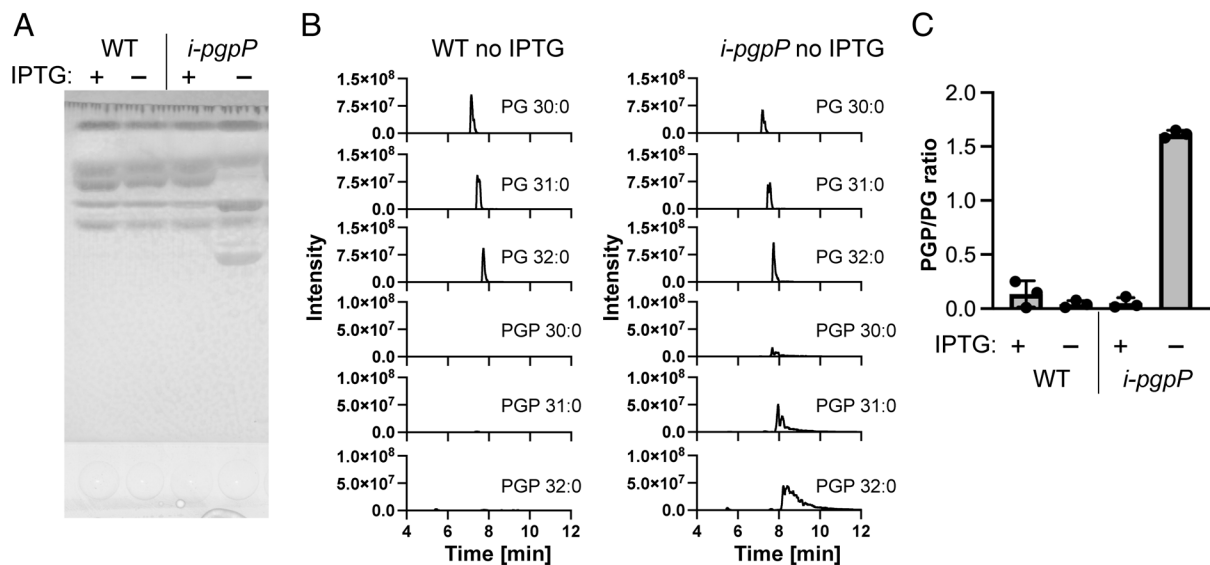


**Fig. 5.** Depletion of PgpP causes an accumulation of PGP in *B. subtilis*. (A) TLC of total lipids extracted from WT *B. subtilis* and the PgpP depletion strain (*i-pgpP*) following growth in LB medium with or without IPTG. The lipids were separated by TLC using an ethylacetate:2-propanol:ethanol:5% ammonia solvent system as described by Osman et al. (30), stained with primulin and the plate imaged. A representative image from three independent experiments is shown. (B) MS traces of PG and PGP. Total membrane lipids isolated from WT or the PgpP depletion strain (*i-pgpP*) grown in LB without IPTG were analyzed by MS in the positive ion mode. Traces for the extracted masses corresponding to PG and PGP lipids with a combined fatty acid carbon chain length of 30:0, 31:0, 32:0 are shown. One representative set of traces from three independent experiments is shown. The complete extracted mass traces are shown in *SI Appendix, Fig. S8*, including traces for lipids isolated from the strains grown in the presence of IPTG. (C) Bar graph of the ratios of PGP/PG in the indicated strains and growth conditions. The area of all PG and PGP peaks as shown in (B) and *SI Appendix, Fig. S8* were integrated, and the average and SD of the PGP/PG ratios from three independent samples were plotted.

Gene neighborhood analysis indicates that in some bacteria within the Bacilli group, *pgpP* co-occurs with other lipid biosynthesis genes including *psaA* and *psd* responsible for phosphatidylserine (PS) and PE lipid synthesis. Furthermore, in several bacteria, including *B. subtilis* and *L. monocytogenes*, a gene encoding a DedA family member with a SNARE-associated domain (PF09335) is present close to *pgpP*. DedA proteins have recently been shown to function as flippases or scramblases of phospholipids and the carrier lipid undecaprenyl phosphate (32, 39–41). Accordingly, the DedA family protein whose gene resides in the same neighborhood as *pgpP* could transport anionic PG phospholipids from the inner to the outer leaflet of the cytoplasmic membrane. The active transport of PG is particularly important in gram-positive bacteria that use PG as a substrate in the synthesis of LTA.

In summary, PgpP is a broadly conserved protein that likely functions as a PGP phosphatase in many bacteria. Its identification completes the Kennedy pathway in *B. subtilis* and probably in a large swath of Firmicutes and Cyanobacteria. Finally, our studies highlight the importance of investigating fundamental biological processes in diverse organisms to uncover how they have developed distinct solutions to the same biochemical problem.

## Materials and Methods

**Bacterial Growth.** Bacterial strains and primers used in this study are listed in *SI Appendix, Tables S5 and S6*. *B. subtilis* and *E. coli* strains were grown in Lysogenic Broth (LB) or LB Agar at 30 °C, 37 °C, 42 °C, or 43 °C as indicated. Antibiotics used for the growth of *E. coli* cultures were 100 µg/mL ampicillin, 30 µg/mL kanamycin, and 10 µg/mL chloramphenicol. Antibiotics for *B. subtilis* growth on agar plates were 10 µg/mL kanamycin, 5 µg/mL chloramphenicol, 1 µg/mL erythromycin and 25 µg/mL lincomycin, 10 µg/mL tetracycline, 16 to 20 µg/mL phleomycin, and 100 µg/mL spectinomycin. *B. subtilis* strains were generated using a one-step competence method. Construction of all strains and plasmids is described as *SI Appendix, Supporting Text*.

***B. subtilis* Growth Curves.** For bacterial growth curves, 4 mL LB medium (where required supplemented with 500 µM IPTG) was inoculated with a freshly streaked

colony of the indicated *B. subtilis* strain. The culture was incubated for 4 h at 37 °C in a roller drum. For *B. subtilis* strains with IPTG inducible gene expression, bacteria from 1 mL of the preculture were collected by centrifugation for 3 min at 6,800 ×g and washed twice with 1 mL LB medium. After the final centrifugation step, the pellet was suspended in 1 mL LB medium and the OD<sub>600</sub> determined. For bacterial growth curves in culture flasks, the bacterial suspensions were diluted to a starting OD<sub>600</sub> of 0.025 in 25 mL LB or LB containing 100 µM IPTG and the cultures were grown with shaking in a 37 °C water bath and OD<sub>600</sub> readings taken at the indicated time points. For growth curves in 96-well plates, 75 µL of the bacterial precultures set to an OD<sub>600</sub> of 0.05 were mixed with 75 µL LB medium. The 96-well plates were incubated at 37 °C with continuous shaking in a Tecan Infinite M Plex plate reader and OD<sub>600</sub> measurements taken every 5 min for the indicated time. For bacterial growth curves with a second back dilution step, 3 mL LB medium supplemented with 500 µM IPTG was inoculated with a colony of the indicated *B. subtilis* strain. The cultures were incubated for 4 h at 37 °C with shaking at which point the bacteria from 1 mL of the preculture were collected by centrifugation for 3 min at 6,200 ×g and washed twice with 1 mL LB medium and subsequently suspended in 1 mL LB medium. Next 3 mL LB medium without or with 100 µM IPTG were inoculated with the washed precultures to an OD<sub>600</sub> of 0.025 and the cultures grown for 3 h at 37 °C with shaking. The cultures were then backdiluted a second time to an OD<sub>600</sub> of 0.025 into 25 mL LB medium without or with 100 µM IPTG. The cultures were grown with shaking in a 37 °C water bath and OD<sub>600</sub> readings taken at the indicated time points. All growth curves were performed with three or more biological replicates. For the growth curves performed in culture flasks, the average readings and SD were plotted. For the growth curves performed in 96-well plates, a representative result was shown.

**Bacterial Plate Spotting Assays.** For *B. subtilis* plate spotting assays, 4 mL precultures were grown for 4 h at 37 °C and washed as described above. The cultures were set to an OD<sub>600</sub> of 0.5 and 10-fold dilutions up to 10<sup>-5</sup> or 10<sup>-6</sup> prepared using LB medium as diluent and 4 µL spotted on LB, LB with 250 µM IPTG or LB with 20 mM xylose plates. The plates were incubated at 30 °C for 17 to 20 h and subsequently imaged. For plate spotting assays with *E. coli*YL24-derived strains containing the empty control plasmid pCB095 or derivatives thereof for expression of the *E. coli* *pgpA*<sub>EC</sub> or *pgpC*<sub>EC</sub>, *S. aureus* *pgpP*<sub>SA</sub> or *B. subtilis* *pgpP*<sub>BS</sub> genes, the strains were grown overnight at 30 °C in 4 mL LB Amp 100 µg/mL, Kan 30 µg/mL Cam 10 µg, and 0.2% L-arabinose. Next day, bacteria from 1 mL culture were collected by centrifugation for 3 min at 10,600 ×g and washed twice

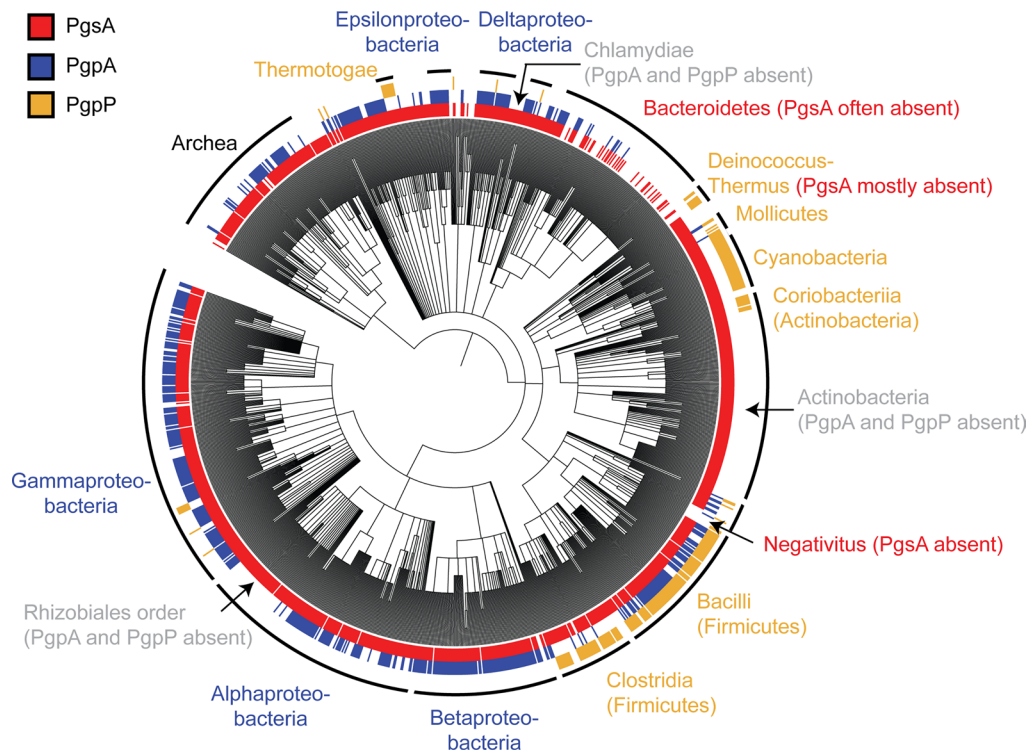


**Fig. 6.** PgpP is broadly conserved in Firmicutes, Cyanobacteria, Mollicutes, Deinococcus-Thermus, and Thermotogae. Phylogenetic tree showing the distribution of PgsA, PgpA, and PgpP homologs in Bacteria and Archaea. The phylogenetic tree was constructed using the Phylo T v2 web site (<http://phylo.t.biobyte.de>) and the 1,187 bacterial and 122 archaeal taxa included in the COG database (33). The taxa in which PgsA (COG0558, shown in red), PgpA (COG1267, shown in blue), and PgpP (YqeG) (COG02179; shown in orange) proteins are found were mapped onto the tree using iTOL V6 (34). Branches with some of the main phyla and classes are indicated on the perimeter of the tree. Phyla and classes in which PgsA homologs are largely absent are shown in red and phyla and classes in which PgpA and PgpP are both absent are shown in gray. PgpP homologs, shown in orange, are found in Firmicutes, Cyanobacteria, Mollicutes, Deinococcus-Thermus, and Thermotogae as well as the class of Coriobacteriia within the Actinobacterium Phylum.

with 1 mL LB medium. The washed cultures were adjusted to an  $OD_{600}$  of 1 and a 10-fold dilution series prepared up to  $10^{-6}$  and 4  $\mu$ L of each dilution spotted onto LB Amp100/Kan30/Cam10/0.2% L-arabinose plates and LB Amp100/Kan30/20 mM xylose plates. The LB Kan30/Amp100/Cam10/0.2% L-arabinose plates were incubated at 30 °C for 40 to 44 h and the LB Amp100/Kan30/20 mM xylose plates were incubated at 42 °C for 19 to 20 h at which point the plates were imaged. All experiments were performed with at least three biological replicates and representative plate images are shown.

**Tn-Seq.** The transposon delivery plasmid pWX642 containing a modified mariner transposon, was introduced into the *B. subtilis* strains PY79 WT (AG101), the *bcrC* mutant strain  $\Delta bcrC::lox72$  (AG289) and the quadruple mutant strain  $\Delta ypqQ::lox72, \Delta yutG::lox72, \Delta pggB::lox72, \Delta bcrC::lox72$  (AG240). 0.5 M to 1 M colonies were pooled for each library as previously described (42). Two independent Tn libraries were constructed for WT and one library was generated for each mutant. Next, gDNA was isolated from the pooled libraries and the samples were prepared for sequencing. The gDNA was cleaved with MmeI, annealed adaptors with barcodes were ligated onto the cut gDNA and the transposon-gDNA junctions amplified in a 19-cycle PCR. The resulting PCR products were pooled, gel extracted, and spiked with 10% Illumina PhiX DNA and sequenced on an Illumina NextSeq instrument using a P1 100 cycle NextSeq kit and recoding the first 35 cycles. The reads were trimmed, mapped onto the *B. subtilis* PY79 genome (NC\_022898) and the number of reads per TA site summed. Next, the number of reads per gene were compared between the WT and mutant strains and significant differences identified using the Mann-Whitney *U* test. The complete dataset is shown as [Dataset S1](#) along with a summary table of the genes that have  $\geq 3\times$  as many insertions in both WT strain datasets compared to the gene in the quadruple mutant strain and with a *P*-value  $\leq 0.05$ . Genes highlighted in yellow in [Dataset S1](#) are deleted in the quadruple mutant strain and hence contain a reduced number of Tn-insertions. Genes highlighted in gray have  $\geq 3$  times as many insertions in both WT strain datasets compared to the gene in the quadruple mutant as well as the *bcrC* single mutant and hence are predicted to be synthetic lethal/sick with *bcrC*. Genes highlighted in green have  $\geq 3$  times as

many insertions in both WT strain datasets compared to the gene in the quadruple mutant but not the *bcrC* single mutant. However, none of these genes codes for a predicted phosphatase.

**Construction of a *S. aureus* gDNA Plasmid Library and Screening for PGP Phosphatase Candidate Enzymes.** For construction of the *S. aureus* gDNA fragment library, the BamHI digested and dephosphorylated pUT18C plasmid was ligated with *S. aureus* RN4220 gDNA partially digested with Sau3AI. The pUT18C-gDNA fragment plasmid library was initially introduced into high-efficiency electrocompetent *E. coli* XL1-Blue cells (Agilent 200228). The obtained transformants were pooled, the plasmid DNA isolated and subsequently introduced by electroporation into *E. coli* strain YL24 pMAK-C and transformants selected on LB Amp100 plates at 43 °C. Transformants were restreaked for single colonies on LB Amp100 plates, and the plates incubated at 37 °C. Next, liquid cultures were prepared from single colonies, the plasmid DNA isolated, and the sequence of the *S. aureus* gDNA fragment determined by Sanger sequencing using forward and reverse plasmid specific primers oANG18\_ABG/pANG19\_ABG. The obtained sequences were mapped onto the *S. aureus* NCTC8325 genome and visualized using SnapGene V7.2.1 and a drawn to scale schematic of some of the mapped reads is shown in [SI Appendix, Fig. S1](#).

**Immunoblot Analysis.** For the preparation of samples for immunoblot analysis, the indicated *B. subtilis* strains were pregrown in 4 mL LB in the presence of 500  $\mu$ M IPTG for 4 h, washed, and subcultured into 25 mL LB in 250 mL culture flasks or 25 mL LB containing 0.4 mM, 1 mM, or 20 mM xylose to a starting  $OD_{600}$  of 0.025. The cultures were incubated with shaking at 37 °C for 3 h at which point bacteria equivalent to 1 mL of  $OD_{600} = 1$  were collected by centrifugation for 5 to 10 min at 10,600  $\times g$ . Bacteria were lysed by incubating them for 15 min at 37 °C in 50  $\mu$ L 10 mM Tris pH7 10 mM MgCl<sub>2</sub> 1 mM EDTA buffer containing 0.4 mg/mL lysozyme, 25 Units DNase I, 0.05 mg/mL RNase, and 1 mM phenylmethylsulfonyl fluoride. Next, the samples were mixed with an equal volume of 2 $\times$  SDS PAGE sample buffer and heated for 5 min at 95 °C. The samples were centrifuged for 5 min at 20,800  $\times g$  and 10  $\mu$ L separated on a 15% PAA gel to detect the

His-tagged proteins or the equivalent of 2.5  $\mu\text{L}$  separated on a 12.5% PAA gel for the detection of the SigA protein. For western-plot analysis the proteins were electrotransferred onto PVDF membranes, blocked for 2 h or overnight in PBS pH 7.4 buffer containing 5% milk and 0.5% Tween 20. The membranes were washed 4 times for 5 min with PBS pH 7.4 containing 0.05% Tween 20 and incubated overnight at 4 °C in 3% w/v BSA in PBS pH 7.4 containing 0.05% Tween 20 with a mouse Anti-His tag antibody (GenScript) at a 1:4,000 dilution or with a rabbit polyclonal SigA antibody at a 1:10,000 dilution. The next day, the membranes were washed 4 times for 5 min with PBS pH 7.4 containing 0.05% Tween 20 and incubated for 2 to 3 h at room temperature with anti-mouse-HRP or anti-rabbit-HRP antibodies at 1:20,000 or 1:4,000 dilutions in 3% (w/v) BSA in PBS with 0.05% Tween 20. The membranes were washed 4 times for 5 min with PBS pH 7.4 with 0.05% Tween 20 and developed using a SuperSignal West Pico PLUS chemiluminescent Substrate (Pierce). The experiment was performed with three biological replicates and a representative result is shown.

**Fluorescence Microscopy.** For the microscopy analysis of early growth phase cultures (3 h after IPTG removal), PY79 and PY79 *i-pgpP*-derived strains with constitutively expressed GFP were pregrown for 4 h in 4 mL LB in the presence of 500  $\mu\text{M}$  IPTG, washed, and back diluted into 25 mL LB or LB with 100  $\mu\text{M}$  IPTG to an  $\text{OD}_{600}$  of 0.0003125 except for the *B. subtilis* strain with inducible *pgpP* expression, which was back diluted to an  $\text{OD}_{600}$  of 0.000625 when grown in LB medium and incubated for 3 h at 37 °C with shaking. For imaging of bacteria from late growth phase cultures (5 h after IPTG removal), cultures were pregrown for 4 h in 4 mL LB in the presence of 500  $\mu\text{M}$  IPTG, washed twice, and back diluted into 25 mL LB medium without IPTG to an  $\text{OD}_{600}$  of 0.025, and incubated for 5 h at 37 °C with shaking. Next, bacteria from the equivalent of 1 mL culture with an  $\text{OD}_{600} = 0.5$  were collected by centrifugation for 3 min at 6,800  $\times g$  and the pellet suspended in 50  $\mu\text{L}$  LB medium containing 5  $\mu\text{M}$  1-(4-trimethylammoniumphenyl)-6-phenyl-1,3,5-hexatriene *p*-toluenesulfonate (TMA-DPH), a lipophilic dye that integrates into the lipid bilayer without any known lipid specificity, and 7.5  $\mu\text{M}$  PI to stain cells with membrane integrity defects. 6  $\mu\text{L}$  of the stained bacterial samples were spotted into 2% LB agarose pads and covered with a #1.5 coverslip and imaged on a fully automated widefield Nikon Ti2-E inverted microscope equipped with a Hamamatsu ORCA-Flash4.0 V3 sCMOS camera, Nikon linear encoded Nikon motorized stage, and a Lumencor Spectra III LED light engine. Phase contrast and fluorescence images were acquired using a Plan Apo 100 $\times$ /1.45 oil immersion objective. The instrument was controlled with Elements 5.2 Acquisition Software. The PI fluorescence signal was detected using a Semrock LED-CFP/YFP/mCherry multipass Dichroic mirror and a Semrock FF01-641/75 emission filter; the TMA-DPH fluorescence signal was detected using an Semrock LED-DAFI/TR/Cy5/Cy7 multipass Dichroic filter and a Semrock FF01-432/36 emission filter. Images were processed using Image J2 Version 2.14.0/1.54f (43). The experiment was performed with two or three biological replicates as indicated in the legend and representative images are shown.

**Lipid Extraction and TLC Analysis.** For the extraction of total phospholipids, precultures of the indicated *B. subtilis* strains were washed and backdiluted to an  $\text{OD}_{600}$  of 0.025 into 100 mL LB medium or 100 mL LB medium containing 100  $\mu\text{M}$  IPTG for the WT or strain *i-pgpP* or 500  $\mu\text{M}$  IPTG for strain *i-pgsA*. The cultures were incubated with shaking in a 37 °C water bath for 2.5 h. At this point, bacteria from the equivalent of 25  $\text{OD}_{600}$  units were collected by centrifugation for 10 min at 4,200  $\times g$ , washed once with 20 mL PBS pH 7.4 buffer, and centrifuged again for 10 min at 4,200  $\times g$ . Subsequently, the wet weight of the bacterial pellet was determined, and the samples were stored at -20 °C until further processing. For the extraction of total membrane lipid, water was added to the bacterial pellet to give a final wet weight of 400 mg and subsequently mixed with 400  $\mu\text{L}$  of 0.2 M HCl and transferred to glass tubes. Next, 2 mL of a 1:1 chloroform:methanol mixture was added and the sample vortexed for 1 min and incubated at RT for 1.5 to 2.5 h and vortexed every 15 to 20 min. The samples were centrifuged for 10 min at 1,500  $\times g$  to remove cell debris and the supernatant transferred to a new glass tube. Next, 1 mL chloroform and 1 mL 0.1 M HCl was added to the sample to give a 1:1:0.9 ratio of chloroform:methanol:0.1 M HCl and resulting in a phase separation. The samples were vigorously vortexed for 1 min and incubated for 10 min at RT and subsequently centrifuged for 10 min at 2,000  $\times g$ . The bottom chloroform phase was transferred to a new vial and dried under a stream

of nitrogen. For TLC analysis, silica gel 60 plates with concentration zones were dried just prior to use for 30 to 60 min in a 100 °C oven, the dried lipid samples were suspended in 100  $\mu\text{L}$  chloroform and 10  $\mu\text{L}$  spotted on the dried TLC plates. The plates were either developed using a 65:25:8 chloroform:methanol:acetic acid solvent system and lipid bands annotated as described in Roney and Rudner (32) or using a 3:9:3:9 ethylacetate:2-propanol:ethanol:5% ammonia solvent system as described by Osman et al. (30). After the TLC run, the plates were dried for a few minutes at room temperature, submerged for 5 to 10 s in a 50  $\mu\text{g}/\text{mL}$  primulin solution in 80% acetone. After drying the plates, they were imaged on a ChemiDoc Touch system (Biorad) using the ethidium bromide filter. The TLC analysis was performed with at least three biological replicates and a representative result is shown.

**Lipid Mass Spectrometry (MS) Analysis.** MS analysis and detection of PG and PGP lipids was performed on a Thermo Vanquish-Orbitrap Exploris 240 liquid chromatography-high-resolution MS system equipped with a Waters Acuity HSS T3 100 Å, 1.8  $\mu\text{m}$  C18, 2.1  $\times$  100 mm column, with guard, using 60:40 acetonitrile:water with 10 mM ammonium formate, 0.1% formic acid (Buffer A), and 90:10 isopropanol:acetonitrile with 10 mM ammonium formate, 0.1% formic acid (Buffer B) at 300  $\mu\text{L}/\text{min}$  and 45 °C. Analytes were separated using a gradient from 30 to 98% B over 10 min followed by wash and equilibration steps. Following TLC analysis, the remaining *B. subtilis* membrane lipids were dried again and suspended in 52  $\mu\text{L}$  methanol and 5  $\mu\text{L}$  injected and run in the positive ion mode. The authentic standard PG C15:0 C18:1-D7 (Avanti Polar Lipids 791640) was analyzed at 10  $\mu\text{g}/\text{mL}$  in methanol and used as a control to identify structure-specific product ions in our MS/MS experiments. The LC-MS analysis was performed on three biological replicates and the masses for PG and PGP lipids with a combined fatty acid carbon chain length of 30:0, 31:0, or 32:0 identified. The peak areas for the mass signal corresponding to these lipids were integrated for each sample separately, and the ratio between PGP and PG lipids was calculated and the average values and SD were plotted. For the LC-MS/MS analysis, the control lipid PG C15:0 C18:1-D7 was used and the experiment was performed once each for the WT PY79 and PY79 *i-pgpP* membrane lipids samples isolated from strains growth in the presence and absence of IPTG.

**Bioinformatics Analysis.** The *E. coli* PgpA (UniProt P18200), PgpB (UniProt P0A924), and PgpC (UniProt P0AD42) protein sequences were used in Domain Enhanced Lookup Time accelerated (DELTA\_BLAST) searchers (22) against the *B. subtilis* 168 genome using the preset standard search parameters. The identified *B. subtilis* hits are listed in [SI Appendix, Table S1](#). Clustal Omega V1.2.4 (44) was used to align the yeast GEP4 (UniProt P38812), *B. subtilis* 168 PgpP (UniProt P54452) and *S. aureus* NCTC8325 PgpP (UniProt Q2FXX9) proteins. The proposed active site aspartic acid residues were annotated based on information provided by Osman et al. (30). For the phylogenetic analysis, information from the clusters of orthologous genes (COGs) database was used, where PgpP (YqeG) and its orthologs are listed under COG2179 and annotated as predicted phosphohydrolase YqeG HAD superfamily (45, 46). The phosphatidylglycerophosphate synthase PgsA is listed under COG0558 and the phosphatidylglycerophosphatase APgpA is listed under COG1267. PhyloT v2 (<https://phylo.t.biobyte.de/index.cgi>) was used for the construction of a phylogenetic tree using the 1,187 bacteria and 122 archaea currently included in the COGs database and the taxa in which one or more PgpP, PgsA, and PgpA orthologs are present were mapped onto the tree using iTOL iTOL V6 (34). For the gene neighborhood analysis, the *B. subtilis* YqeG protein sequence (BSU\_25680) was used in Blast searchers (47, 48) using the RefSeq Selected proteins (refseq\_select) database and performing separate BlastP searches against the following Phyla and orders (Bacilli taxid:91061). The standard preset search parameters were used except that the searches were expanded to the top 5,000 hits. The obtained sequences were uploaded to the Enzyme Function Initiative web site and an SNN file generated, which was subsequently used for the Gene Neighborhood analysis to determine how conserved the operon structure is in bacteria (49, 50).

**Data, Materials, and Software Availability.** Raw Tn-seq Illumina sequence files have been deposited in the Sequence Read Archive at the National Center for Biotechnology Information under BioProject ID [PRJNA1153456](https://www.ncbi.nlm.nih.gov/bioproject/PRJNA1153456) (51).

**ACKNOWLEDGMENTS.** We thank all the members of the Bernhardt-Rudner supergroup for helpful advice, discussions, and encouragement and the students

and teaching assistants and other instructors who took part in the 2022 and 2023 Cold Spring Harbor Advanced Bacterial Genetics (ABG) course for their effort in generating the *S. aureus* gDNA plasmid library and performing the initial screen using the *E. coli* YL24 pMAK-C strain. We are very grateful to the late Chris Raetz for sharing *E. coli* strain YL24 pMAK-C. We would also like to acknowledge the support of the Analytical Chemistry Core at Harvard Medical School where the

MS analysis was performed and members of the MicRoN core facility at Harvard Medical School (RRID: SCR 022209) for training and support. A.G. performed virtually all the experiments in this study during her sabbatical year in the Bernhard and Rudner labs. Support for this work comes from the Leverhulme Trust International Fellowship IF-2023-026 (A.G.), the NIH Grants R35GM145299 (D.Z.R.), R01 AI083365 (T.G.B.), and U19 AI158028 (T.G.B. and D.Z.R.).

1. E. P. Kennedy, Sailing to Byzantium. *Annu. Rev. Biochem.* **61**, 1–28 (1992).
2. W. Dowhan, M. Bogdanov, P. Eugene, Kennedy's legacy: Defining bacterial phospholipid pathways and function. *Front. Mol. Biosci.* **8**, 666203 (2021).
3. A. Gründling, O. Schneewind, Genes required for glycolipid synthesis and lipoteichoic acid anchoring in *Staphylococcus aureus*. *J. Bacteriol.* **189**, 2521–2530 (2007).
4. A. Gründling, O. Schneewind, Synthesis of glycerol phosphate lipoteichoic acid in *Staphylococcus aureus*. *Proc. Natl. Acad. Sci. U.S.A.* **104**, 8478–8483 (2007).
5. L. I. Salzberg, J. D. Helmann, Phenotypic and transcriptomic characterization of *Bacillus subtilis* mutants with grossly altered membrane composition. *J. Bacteriol.* **190**, 7797–7807 (2008).
6. J. D. Nickels *et al.*, *Bacillus subtilis* lipid extract, a branched-chain fatty acid model membrane. *J. Phys. Chem. Lett.* **8**, 4214–4217 (2017).
7. J. R. Willdigg, J. D. Helmann, Mini review: Bacterial membrane composition and its modulation in response to stress. *Front. Mol. Biosci.* **8**, 634438 (2021).
8. J. B. Parsons, C. O. Rock, Bacterial lipids: Metabolism and membrane homeostasis. *Prog. Lipid Res.* **52**, 249–276 (2013).
9. K. Kobayashi *et al.*, Essential *Bacillus subtilis* genes. *Proc. Natl. Acad. Sci. U.S.A.* **100**, 4678–4683 (2003).
10. M. Hashimoto *et al.*, Induction of extracytoplasmic function sigma factors in *Bacillus subtilis* cells with membranes of reduced phosphatidylglycerol content. *Genes Genet. Syst.* **84**, 191–198 (2009).
11. C. Miyazaki, M. Kuroda, A. Ohta, I. Shibuya, Genetic manipulation of membrane phospholipid composition in *Escherichia coli*: *PgsA* mutants defective in phosphatidylglycerol synthesis. *Proc. Natl. Acad. Sci. U.S.A.* **82**, 7530–7534 (1985).
12. Y. M. Zhang, C. O. Rock, Membrane lipid homeostasis in bacteria. *Nat. Rev. Microbiol.* **6**, 222–233 (2008).
13. T. Icho, C. R. Raetz, Multiple genes for membrane-bound phosphatases in *Escherichia coli* and their action on phospholipid precursors. *J. Bacteriol.* **153**, 722–730 (1983).
14. Y. H. Lu, Z. Guan, J. Zhao, C. R. Raetz, Three phosphatidylglycerol-phosphate phosphatases in the inner membrane of *Escherichia coli*. *J. Biol. Chem.* **286**, 5506–5518 (2011).
15. M. El Ghachi, A. Derbise, A. Bouhss, D. Mengin-Lecreulx, Identification of multiple genes encoding membrane proteins with undecaprenyl pyrophosphate phosphatase (UppP) activity in *Escherichia coli*. *J. Biol. Chem.* **280**, 18689–18695 (2005).
16. H. Zhao *et al.*, Depletion of undecaprenyl pyrophosphate phosphatases disrupts cell envelope biogenesis in *Bacillus subtilis*. *J. Bacteriol.* **198**, 2925–2935 (2016).
17. M. E. Ghachi *et al.*, Crystal structure and biochemical characterization of the transmembrane PAP2 type phosphatidylglycerol phosphate phosphatase from *Bacillus subtilis*. *Cell Mol. Life Sci.* **74**, 2319–2332 (2017).
18. M. Santiago *et al.*, A new platform for ultra-high density *Staphylococcus aureus* transposon libraries. *BMC Genomics* **16**, 252 (2015).
19. M. A. Fischer *et al.*, *Listeria monocytogenes* genes supporting growth under standard laboratory cultivation conditions and during macrophage infection. *Genome Res.* **32**, 1711–1726 (2022).
20. M. S. Gilmore *et al.*, Genes contributing to the unique biology and intrinsic antibiotic resistance of *Enterococcus faecalis*. *mBio* **11**, e02962–20 (2020).
21. T. van Opijnen, K. L. Bodi, A. Camilli, Tn-seq: High-throughput parallel sequencing for fitness and genetic interaction studies in microorganisms. *Nat. Methods* **6**, 767–772 (2009).
22. G. M. Boratyn *et al.*, Domain enhanced lookup time accelerated BLAST. *Biol. Direct* **7**, 12 (2012).
23. R. Bernard, M. El Ghachi, D. Mengin-Lecreulx, M. Chippaux, F. Denizot, BcrC from *Bacillus subtilis* acts as an undecaprenyl pyrophosphate phosphatase in bacitracin resistance. *J. Biol. Chem.* **280**, 28852–28857 (2005).
24. J. Radeck, N. Lautenschlager, T. Mascher, The essential UPP phosphatase pair BcrC and UppP connects cell wall homeostasis during growth and sporulation with cell envelope stress response in *Bacillus subtilis*. *Front. Microbiol.* **8**, 2403 (2017).
25. T. Pedreira, C. Eilmann, J. Stülke, The current state of SubtiWiki, the database for the model organism *Bacillus subtilis*. *Nucleic Acids Res.* **50**, D875–D882 (2022).
26. A. Terakawa *et al.*, *Bacillus subtilis* 5'-nucleotidases with various functions and substrate specificities. *BMC Microbiol.* **16**, 249 (2016).
27. J. Jumper *et al.*, Highly accurate protein structure prediction with AlphaFold. *Nature* **596**, 583–589 (2021).
28. M. Varadi *et al.*, AlphaFold Protein Structure Database in 2024: Providing structure coverage for over 214 million protein sequences. *Nucleic Acids Res.* **52**, D368–D375 (2024).
29. M. van Kempen *et al.*, Fast and accurate protein structure search with Foldseek. *Nat. Biotechnol.* **42**, 243–246 (2024).
30. C. Osman, M. Haag, F. T. Wieland, B. Brugger, T. Langer, A mitochondrial phosphatase required for cardiolipin biosynthesis: The PGP phosphatase Gcp4. *EMBO J.* **29**, 1976–1987 (2010).
31. A. Seifried, J. Schultz, A. Gohla, Human HAD phosphatases: Structure, mechanism, and roles in health and disease. *FEBS J.* **280**, 549–571 (2013).
32. I. J. Roney, D. Z. Rudner, The DedA superfamily member PetA is required for the transbilayer distribution of phosphatidylethanolamine in bacterial membranes. *Proc. Natl. Acad. Sci. U.S.A.* **120**, e2301979120 (2023).
33. R. L. Tatusov, M. Y. Galperin, D. A. Natale, E. V. Koonin, The COG database: A tool for genome-scale analysis of protein functions and evolution. *Nucleic Acids Res.* **28**, 33–36 (2000).
34. I. Letunic, P. Bork, Interactive Tree of Life (iTOL) v6: Recent updates to the phylogenetic tree display and annotation tool. *Nucleic Acids Res.* **52**, W78–W82 (2024).
35. C. H. Hung, K. Kobayashi, H. Wada, Y. Nakamura, Isolation and characterization of a phosphatidylglycerophosphate phosphatase 1, PGPP1, in *Chlamydomonas reinhardtii*. *Plant Physiol. Biochem.* **92**, 56–61 (2015).
36. Y. Zhou *et al.*, Identification and characterization of a plastidial phosphatidylglycerophosphate phosphatase in *Arabidopsis thaliana*. *Plant J.* **89**, 221–234 (2017).
37. Y. C. Lin, K. Kobayashi, C. H. Hung, H. Wada, Y. Nakamura, Arabidopsis phosphatidylglycerophosphate phosphatase 1 involved in phosphatidylglycerol biosynthesis and photosynthetic function. *Plant J.* **88**, 1022–1037 (2016).
38. Y. C. Lin, K. Kobayashi, H. Wada, Y. Nakamura, Phosphatidylglycerophosphate phosphatase is required for root growth in *Arabidopsis*. *Biochim. Biophys. Acta Mol. Cell Biol. Lipids* **1863**, 563–575 (2018).
39. I. J. Roney, D. Z. Rudner, Two broadly conserved families of polyprenyl-phosphate transporters. *Nature* **613**, 729–734 (2023).
40. H. Todor, N. Herrera, C. A. Gross, Three bacterial DedA subfamilies with distinct functions and phylogenetic distribution. *mBio* **14**, e0002823 (2023).
41. B. Sit *et al.*, Undecaprenyl phosphate translocases confer conditional microbial fitness. *Nature* **613**, 721–728 (2023).
42. G. S. Dobihal, J. Flores-Kim, I. J. Roney, X. Wang, D. Z. Rudner, The WalR-WalK signaling pathway modulates the activities of both CwlO and LytE through control of the peptidoglycan deacetylase PdaC in *Bacillus subtilis*. *J. Bacteriol.* **204**, e0053321 (2022).
43. C. T. Rueden *et al.*, ImageJ2: ImageJ for the next generation of scientific image data. *BMC Bioinformatics* **18**, 529 (2017).
44. F. Madeira *et al.*, The EMBL-EBI Job Dispatcher sequence analysis tools framework in 2024. *Nucleic Acids Res.* **52**, W521–W525 (2024), 10.1093/nar/gkae241.
45. R. L. Tatusov, E. V. Koonin, D. J. Lipman, A genomic perspective on protein families. *Science* **278**, 631–637 (1997).
46. M. Y. Galperin, K. S. Makarova, Y. I. Wolf, E. V. Koonin, Expanded microbial genome coverage and improved protein family annotation in the COG database. *Nucleic Acids Res.* **43**, D261–269 (2015).
47. S. F. Altschul *et al.*, Gapped BLAST and PSI-BLAST: A new generation of protein database search programs. *Nucleic Acids Res.* **25**, 3389–3402 (1997).
48. S. F. Altschul *et al.*, Protein database searches using compositionally adjusted substitution matrices. *FEBS J.* **272**, 5101–5109 (2005).
49. R. Zallot, N. Oberg, J. A. Gerlt, The EFI web resource for genomic enzymology tools: Leveraging protein, genome, and metagenome databases to discover novel enzymes and metabolic pathways. *Biochemistry* **58**, 4169–4182 (2019).
50. N. Oberg, R. Zallot, J. A. Gerlt, EFI-EST, EFI-GNT, and EFI-CGFP: Enzyme function initiative (EFI) web resource for genomic enzymology tools. *J. Mol. Biol.* **435**, 168018 (2023).
51. A. Gründling, ANG20240214\_Bacillus\_subtilis\_TnSeq. NIH NCBI. <https://www.ncbi.nlm.nih.gov/sra/?term=PRJNA1153456>. Deposited 28 August 2024.